Correlation of Dielectric and Magnetic Properties in Cobalt Zinc Ferrite

Dhiren K. Pradhan[1,a)], Shalini Kumari[1], Venkata S. Puli[2], Proloy T. Das[3], Dillip K. Pradhan[4], Ashok Kumar[5], J. F. Scott[6], and Ram S. Katiyar[1, a)]

[1] *Department of Physics and Institute of Functional Nanomaterials, University of Puerto Rico, San Juan-00936, PR, USA*
[2] *Department of Physics and Engineering Physics, Tulane University, New Orleans, LA-70118, USA.*
[3] *Department of Physics, Indian Institute of Technology, Kharagpur-721302, India.*
[4] *Department of Physics& Astronomy, National Institute of Technology, Rourkela-769008, India.*
[5] *National Physical Laboratory (CSIR), Delhi, India.*
[6] *Department of Chemistry and Department of Physics, University of St. Andrews, St. Andrews KY16 ST, United Kingdom*

Abstract

Multiferroic composite structures, i.e., composites of magnetostrictive and piezoelectric materials can be envisioned towards the goal of achieving strong room-temperature ME coupling for real practical device applications. Magnetic materials with high magnetostriction, high Néel temperature (T_N), high resistivity and large magnetization are required to observe high ME coupling in composite structures. In continuation to our investigations for suitable magnetic candidate for multiferroic composite structures, we have studied the crystal structure, dielectric, transport, and magnetic properties of $Co_{0.65}Zn_{0.35}Fe_2O_4$ (CZFO). Rietveld refinement of X-ray diffraction patterns confirms the phase purity with cubic crystal structure with ($Fd\bar{3}m$) space group; however, we have found a surprisingly large magnto-dielectric anomaly at the Neel temperature, unexpected for a cubic structure. The presence of mixed valences of Fe^{+2}/Fe^{+3} cations is probed by X-ray photon spectroscopy (XPS), which support the catonic ordering-mediated large dielectric response. Large dielectric permittivity dispersion with a broad anomaly is observed in the vicinity of the magnetic phase transition temperature (T_N) of CZFO suggest the strong correlation

between dielectric and magnetic properties. The ferromagnetic-paramagnetic phase transition of CZFO has been found ~640 K, which is well above room temperature. CZFO exhibits low loss tangent, high dielectric constant and large magnetization with soft magnetic behavior above room temperature. We describe the possible potential candidates for multiferroic composite structures as well as for multifunctional and spintronics device applications.

Key words: Ferrimagnetic, Multiferroics, Dielectric [a)] Author to whom correspondence to be addressed. Electronic mail: rkatiyar@hpcf.upr.edu (Ram S. Katiyar), dhirenkumarp@gmail.com (Dhiren K. Pradhan).

Introduction

Magnetic materials have attracted considerable attention with intensive research and development due to their remarkable high electronic and magnetic properties, and they have been widely used as electro-optic devices, ferrofluid-based rocket fuel, microwave devices, and in high-density information storage, magneto-optic recording and magnetic resonance imaging, drug delivery systems, etc..[1,2,3,4,5] Among magnetic materials, ferrimagnets are often high Curie-temperature (T_C) magnetic insulators having non-zero magnetic moment along with spin-dependent band gaps that can be utilized in spintronics as well as in spin-caloritronics.[6,7] The scarcity of room temperature single-phase multiferroics due to the frequent chemical incompatibility between magnetism and ferroelectricity, low magnetic critical temperatures, and/or weak magnetoelectric (ME) coupling have led researchers to the design and development of artificial composite structures with magnetic components as insulating ferrimagnetic materials.[8,9,10,11] The combination of spinel ferrites with high magnetostriction, high resistivity, high magnetic phase transition temperature, and structural compatibility with ferroelectric perovskites has already proven to provide important strain-driven magnetoelectric magnetic field sensor devices.[9,12,13,14] It is also known that the

magnetic and electrical properties of the ferrites can be substantially manipulated by the substitution of non-magnetic ions. With the substitution of Cu, Zn, and Cr at A-sites, Ni and Co ferrites usually have been found to increase their electrical resistivity.[9,15] Cobalt zinc ferrite (CZFO) is a soft magnetic material having high saturation magnetization, low coercivity, high resistivity, high magnetostriction coefficient and low dielectric loss, thus making it an attractive ferrimagnetic candidate for composite multiferroics.[1,16,17,18,19] In the case of ferrites, the dielectric permittivities are increased due to the hopping of electrons or polarons between cationic sites. The oxidation states of cations and the cation distribution play a major role in the conduction process of ferrites. Hence the origin of high dielectric permittivity around the Neel temperature in CZFO needs to be investigated. When a conduction electron or polaron interacts with the magnetic moment of a transition metal ion, the coupling is best described by a spin-polaron model. In the present work we show a surprisingly strong magneto-dielectric anomaly at the Neel temperature in CZFO, despite the fact that it is of globally cubic symmetry.

Cobalt ferrites doped with various percentages of Zn exhibit multifunctional properties; therefore an in-depth understanding of the correlation of polarization and electrical conduction with spin dynamics is of great importance from both a fundamental and a technological point of view. The optimized ratio $Co_{0.65}Zn_{0.35}Fe_2O_4$ has been chosen for the present investigation since it exhibits highest saturation magnetization with high magnetostriction in the entire cobalt – zinc series, having a high Curie temperature.[17,18,19] In this report the correlation between the dielectric and magnetic behavior with the origin of high dielectric constant has been studied.

Experimental Details

The polycrystalline samples of ceramic $Co_{0.65}Zn_{0.35}Fe_2O_4$ were synthesized by a high-temperature solid-state reaction route using high-purity (99.9%) oxide precursors CoO, ZnO

and Fe_2O_3 in required stoichiometry. These ingredients were mixed with methanol, calcined at an optimized temperature of 1350^0C for 6 hours, and pelletized with a final sintering at 1400ºC for 10 h based on the literature available.[18] X-ray diffractometer (Rigaku Ultima III) was used to check the phase formation of the bulk samples equipped with CuKα (λ = 1.54 Å) radiation source operating in the Bragg–Brentano geometry. The Rietveld structure refinement was performed on experimental XRD data using FullProf Suite software. Scanning electron microscopy (SEM) images were collected with the help of a JEOL JSM-6480LV system. The temperature dependent dielectric parameters: capacitance, dissipation factor, impedance, and phase angles, were measured using an impedance analyzer HP4294A with MMR Technologies K-20 programmable temperature controller for fixed ac voltage amplitude of 0.5 V in a wide frequency range of 100 Hz to 1 MHz. The elemental analysis of fabricated pellets was done via high-resolution X-ray photoemission spectroscopy (XPS). Magnetic properties of the samples were measured using a Quantum design PPMS Dynacool in a wide range of temperature 300 -800 K.

Results and Discussion

Figure 1 shows the room temperature characteristic XRD patterns with sharp and well defined peaks that illustrate the spinel structure. Impurity phases have not been detected in samples within the experimental XRD error limit, indicating the high quality of the synthesized material. In order to have a better understanding of structural parameters of CZFO with spinel phase (quantitatively and qualitatively), we have refined the experimental XRD patterns using a FULLPROF package with space group ($Fd\bar{3}m$). There is a close agreement between the experimental (symbols) and simulated data with a satisfactory chi square value 1.648. We have taken care of many parameters, such as background, zero shift, specimen displacement, atomic positions, thermal factors, scale factor, lattice parameters, FWHM, and shape parameters during refinement. The lattice parameter of CZFO is found to

be 8.4183 Å from the refinement, which matches well with previous reports.[19,20] Using the obtained unit cell parameters and atomic positions, a three-dimensional sketch of the CZFO unit cell projected along the c-axis is shown in Figure 1(b). The inset of Figure 1(a) shows the surface topography image of a CZFO sintered pellet, which displays densely packed grains with few scattered pores and voids. Distinct micron-sized grains and related grain boundaries are clearly visible, homogenously distributed throughout the matrix.

For the further investigation of formation of the material and cation disorder, Raman spectroscopic measurements have been performed at room temperature. Raman spectroscopy is a sensitive and nondestructive technique to investigate the complex structure of strongly correlated electron systems such as ferroelectric, magnetic and multiferroic materials with compositional and structural disorder. As stated above, the crystal structure of CZFO is cubic with $Fd\bar{3}m$ space group symmetry and the unit cell contains 56 atoms. The smallest Bravais cell in this symmetry consists of 2 formula units with 14 atoms. The group theory analysis of $Fd\bar{3}m$ crystal symmetry with cubic structure predicts zone centre phonons by the following irreducible representations:

$$\Gamma = A_{1g}(R) + E_g(R) + T_{1g} + 3T_{2g}(R) + 2A_{2u} + 2E_u + 4T_{1u}(IR) + 2T_{2u} \quad \ldots\ldots\ldots\ldots\ldots\ldots\ldots\ldots\ldots\ldots (1)$$

Here R and IR represent Raman and Infrared active modes respectively.

There are five first-order Raman active modes ($A_{1g} + E_g + + 3T_{2g}$) expected in ferrites at ambient conditions. All five observed modes i.e E_g, T_{2g} (1), T_{2g}(2), A_{1g} (1) and A_{1g} (2) have been assigned based on the previous reports. In spinel ferrites it is well known that the modes above 600 cm^{-1} belong to the motion of the oxygen atoms in tetrahedral AO_4 groups, whereas frequencies below 600 cm^{-1} belong to the motion of the oxygen atoms in octahedral BO_6 group. The schematic diagram shown in Figure 2(a) representing the unit cell along with the FeO_6 octahedral and BO_4 tetrahedral sites of CZFO. The Raman spectra of pure $CoFe_2O_4$ and

CZFO are shown in Figure 2(b). Lorentzian peak functions have been used to fit all of the observed Raman modes, and the Raman spectra can be best fitted by five distinct peaks. It is observed that the peak positions of the $T_{2g}(1)$, $T_{2g}(2)$ and A_{1g} of CZFO show significant red shift compared to pure $CoFe_2O_4$. As indicated above, the peaks of A_{1g} symmetry belong to the motion of oxygen atoms in the tetrahedral AO_4 group. In our case Zn has been substituted in Co in the A site. Hence it is expected that the phonon frequencies related to A site oxygen atom (i.e. those of A_{1g} symmetry) should be red shifted (as Zn has higher atomic mass and ionic radii than Co). However, it is also found that some of the peaks related to oxygen motion (T_{2g} (1) and T_{2g} (2)) associated with B site (Fe) show noticeable red-shift. The possible reason of the observed red shift of T_{2g} (1) and T_{2g} (2) could be due to the high temperature sintering of CZFO to get the pure phase. It is evident that at such high temperature, Zn vacancies are formed in the crystal lattice. To compensate the loss of Zn, some of the Fe^{3+} ions from the B site reduce to Fe^{2+} ions which eventually hop to the Zn site. After hopping of the central Fe ions to A sites from their initial stable configurations, the local system will no longer be in equilibrium with its neighbors. In order to stabilize the new position of the ions, other surroundings ions have to move accordingly. This hopping process will have significant impact on the vibrational frequencies of normal modes of the associated octahedral BO_6 site. The proposed hopping process is also supported from XPS and conductivity studies which will be discussed in the following sections. Note that this hopping of ions causes the existence of both Fe^{2+} and Fe^{3+} in the matrix which increases dielectric permittivity.

Figure 3(a) shows the variation of relative dielectric permittivity (ε_r) and loss tangent ($\tan\delta$) as functions of temperatures and frequencies. The magnitude and dispersion of dielectric permittivity remain nearly constant up to 500 K, and thereafter increase with increase in temperature. The dielectric constant and loss tangent are sensitive to probe

frequencies, where low frequencies (<10 kHz) significantly influence the nature and magnitude of the dielectric constant with increase in temperature. In general the dielectric permittivity in solids is mainly due to four type of polarizations: (i) space charge/interfacial polarization at grain boundaries and electrodes; (ii) dipolar polarization, such as that due to neighboring Fe^{+2}/Fe^{+3} ion pairs; (iii) atomic polarization (shifts of single ions, due to strain or vacancies; and (iv) electronic polarization.[21,22] The interfacial and dipolar polarization are strongly temperature dependent under the present probe range of frequencies. The CZFO suffers Zn loss during high temperature sintering and calcination, resulting in vacancies and partially charged oxygen ions; electrons at oxygen sites will bond with the neighboring Fe^{3+} ions, which gives rise to Fe^{2+} ions.[23,24] Hence due to the high-temperature synthesis process, both Fe^{2+} and Fe^{3+} naturally develop in the matrix, which is further confirmed by our XPS analysis. The existence of Fe^{2+} cations and oxygen anions gives rise to excess thermally activated mobile charge carriers which hop among various charge-trap sites.[25] As a result, Fe^{2+} and Fe^{3+} form a dipole-type polarization, which significantly increase the dielectric permittivity. So the dielectric permittivity increases due to the hopping of thermally activated charge carriers.[23] Active hopping among the polarons and electrons becomes frozen in at low temperatures, significantly lowering dielectric loss and electric conductivity. The electron hopping is activated with increase in temperature by lattice vibrations, leading to polaron hopping.[21] These factors lead to the increase in the dielectric constant and loss with increase in temperature. This behavior is well correlated with the variation of the polarizability obtained from frequency dependent ac conductivity of this material which will be discussed below (in particular, A(T), the coefficient in the equation below). We note that ε_r increases gradually with increase of temperature to its maximum value and then decreases. This is wholly unexpected and not due to ordinary thermal effects. We find a broad anomaly at 600-700 K. A broad ferrimagnetic transition also has been observed in this temperature range,

which suggests there is a strong spin-polaron coupling in this material. The further confirmation of this spin-polaron coupling is discussed below in terms of the temperature dependent conductivity and magnetic behavior.

In order to clarify the origin of such high dielectric constant in CZFO, the variation of dielectric constant with frequency (log-log scale) throughout the temperature range of investigation is depicted in Figure 3(b). At low temperature there is a strong dispersion in the dielectric constant followed by weak dielectric relaxation behavior. The weak relaxation behavior is found to be above 100 kHz at 80 K and the peak of the relaxation behavior shifted towards the high frequency side with increase in temperature; for higher temperatures it is going beyond the window of the frequency range of investigation. In the high temperature regime the frequency dependent dielectric spectra are also characterized by step-like relaxation behavior in the low frequency region. This step-like behavior-shifts towards the high frequency side with increase in temperature. The step like behavior in the low frequency region along with the high frequency dispersion region is observed in many high dielectric constant materials such as CCTO.[26] The dielectric dispersion, step-like behavior in frequency dependent dielectric properties and the high tangent loss in the low frequency region can be attributed to interfacial/space charge polarization of the materials.[22] Assuming the CZFO material is a heterogeneous electrical microstructure with grain and grain boundary having different electrical conductivity, the frequency dependent dielectric behavior can be explained on the basis of Maxwell-Wagner theory of interfacial polarization in consequence with the Koops' phenomenological theory.[27] According to Koops' theory in conjunction with the classical brick layer model (BLM), the grain and grain boundary are supposed to have different conductivities and to be connected in series with each other, which gives rise to high dielectric constant and step-like dispersion. In fact in the ferrite systems, this conductivity inhomogeneity due to grain and grain boundary gives rise to different charge hopping process

i.e., different hopping process due to grain and grain boundary. So the collective mechanism such as conductivity in homogeneity leading to different hopping processes and accumulation of charge carriers at the boundaries, leading to the high dielectric constant and steps in frequency dependent dielectric properties.[28]

In order to verify the presence of grain and grain boundary contribution to the observed high dielectric constant in CZFO, complex impedance spectra (Nyquist-plots) at different temperatures are shown in Figure 3(c). The Nyquist plot normally comprises a single semicircular arc at low temperatures with center often below the real axis suggesting the departure from ideal Debye nature (CPE – constant phase elements). At low temperatures (up to 440 K) one semicircular arc has been observed, whereas at higher temperatures two semicircular arcs have been observed. The two observed overlapping semicircular arcs at high temperatures are due to the contribution of the grain (bulk) and grain boundary to the electrical properties of CZFO. It is well known that an equivalent circuit can be used in impedance spectroscopy analysis to establish the structure-property relationship of materials. Here, up to 440 K, one semicircular arc of the impedance spectra has been modeled to an equivalent circuit of a resistance (grain resistance) and a CPE connected in parallel. Above 440 K, two overlapping semicircular arcs of the impedance spectra have been modeled to an equivalent circuit containing (i) a resistance (grain resistance) and a CPE connected in parallel, (iii) a parallel combination of a resistance (grain boundary resistance) and a CPE and all these connected in series. Figure 3(c) shows the Nyquist plots (symbols) with fitted data (solid line) utilizing ZSimp Win Version 2 software for CZFO at various temperatures. We found a close agreement between the experimental and fitted data which verify the correctness of choosing the circuit.

It can be further noted that the dielectric constant of CZFO found to be higher due to the large grain size. For higher grain size there exist large differences between the grain and

the grain boundary resistances, which increase the polarization and hence dielectric constant. As can be seen from the SEM micrograph, the grain size is large (5–10 μm) due to higher sintering temperature, which might be one reason for high dielectric constant observed in CZFO.

In order to understand the origin of enhanced dielectric constant of these samples further, high-resolution XPS measurements have been carried out to determine the oxidation state of Co, Fe, Zn and O. Photoelectron characteristic peaks of Co $2p_{3/2}$(781.03), Co $2p_{1/2}$(796.53), Zn $2p_{3/2}$ (1021.7), Zn $2p_{1/2}$ (1044.7), Fe $2p_{3/2}$(710.78), Fe $2p_{1/2}$(724.38), and O 1*s* (530.30) were observed in the high-resolution XPS spectra, which are in agreement with reported values.[29] The Fe $2p_{3/2}$ structure can be deconvoluted into two peaks that confirm the existence of two valence states of Fe elements (Fe^{2+} and Fe^{3+}) in CZFO, as shown in Figure 3(d). The inset of Figure 3(d) shows the full XPS spectra of Fe with two satellite peaks. The coexistence of Fe^{2+} and Fe^{3+} occurs because of the cation vacancies and partially charged oxygen ions due to the loss of Zn during high temperature synthesis. As a consequence, occurrence of Fe2*p* ions gives rise to electron hopping between the Fe ions in +2 and +3 states. The coexistence of Fe^{2+} and Fe^{3+} dipoles results in orientational polarization, which is one probable reason of enhancement of dielectric constant. In our case the Fe^{3+} ions predominate at lower temperature, contributing to the increase of dielectric constant with temperature.[21,22,23]

Figure 4(a) shows the variation of ac conductivity with frequency at different temperatures. The ac electrical conductivity (σ_{ac}) has been calculated from the dielectric data using the empirical relation; $\sigma_{ac} = \omega\varepsilon_r\varepsilon_0\tan\delta$, where ω, ε_0, ε_r, and $\tan\delta$ are angular frequency, permittivity in free space, relative permittivity, and loss tangent, respectively.[22] At low temperature (below 240 K), ac conductivity increases with increase in frequency throughout the frequency range of investigation. At higher temperatures the ac conductivity spectra are

characterized by the appearance of a frequency-independent plateau at lower frequencies and frequency dispersion at higher frequencies, (ω^n dependence of conductivity). This type of frequency dependent conductivity spectra in general can be explained by Jonscher's power law[30], governed by the equation $\sigma_{ac}= \sigma_{dc} +A(T)\omega^n$. Here σ_{dc} is the dc conductivity (frequency independent plateau in the low frequency region); A(T), the temperature dependent frequency pre-exponential factor; and n, the power law exponent which generally varies between 0 and 1. We have fitted the ac conductivity spectra using Jonscher's single power law, and there is a close agreement between experimental and fitted data, as shown in the inset of Figure 4(a) for 80 K as typical. The conductivity spectra have been fitted for all temperatures, and the fitted parameters σ_{dc}, A, and n are plotted versus temperature. Actually n should equal to 0 if the carriers are free to drift through the ceramic body. As in our case n values varies from 0.5 to 0.9, which clearly indicates that the motion of these charges leads to not only due to conduction but also to considerable polarization. It is a typical feature of localized polarons in most disordered systems. These polarons move with the polarization induced.[27,29]

Figure 4(b) shows the variation of A and n as a function of temperature. It has been observed that the value of n decreases slowly with increase in temperature up to 500 K and thereafter decreases rapidly near the magnetic phase transition temperature. In contrast, the behavior of the A is completely opposite to the behavior of n: with increase in temperature the value of A is nearly constant up to 500 K and thereafter suddenly increases. The degree of interaction between the mobile ions with the lattice is represented by the exponent n, where n=1 implies pure Debye-type dielectric behavior, and where the interaction between the neighboring dipoles is almost negligible: i.e., the charge carriers are free to migrate through the ceramic body.[31] At low temperatures the interactions between the mobile ions are negligible as the value of n is around 0.9. With increase in temperature the value of n is almost constant up to ~ 500 K and then decreases sharply to 0.5 which indicates that the

interaction increases, presumably due to some disorder. The fitted value of n was found to be nearly 0.5 in the temperature range of 500 to 700 K, which implies fast hopping mobile charge carriers and random distributions of localized charge states. This indicates that the mobility of the charge carriers not only enhances the conduction but also considerably increases the polarization. This type of behavior has been observed in disorder systems due to localized polarons.[32,33] The temperature dependent n-plot and magnetization-temperature plot follow a similar trend: n(T) and magnetic moment drop drastically in the temperature range of 500-700 K, which suggests strong phonon-magnon interactions. The pre-exponential factor A(T) determines the strength of the polarizability.[34] The increase in the value of A(T) with increase in temperature establishes the increase in polarizability and hence dielectric properties. The temperature dependent behavior of A is quite similar to the variation of the temperature dependent dielectric properties.

The variation of dc conductivity (obtained after fitting the ac conductivity spectra) with inverse temperature is shown in inset of Figure 4(b). With increase in temperature the dc conductivity increases slowly up to 400 K, thereafter increasing rapidly. The temperature dependent conductivity can be divided into two regions having different slopes. We have calculated the activation energy from the plot above. The values of activation energy for high and low temperatures are found to be E_a = 0.25 eV and 0.03 eV, respectively, suggesting an active role of interfacial activated electronic charge carriers in the conduction process which has been explained on the basis of small polaron hopping.[21,22,23,29]

The observed behavior of high dielectric constant around transition temperature can be explained by a spin-polaron model. According to this equation, the total energy

$$E_S = \frac{5\hbar^2\pi^2}{6m}\left(\frac{4mJ_2}{\hbar^2\pi a^3}\right)^{2/5} - J_1 \quad \ldots\ldots(2)$$

where m is the mass of the electron; a, the lattice parameter; J_1, the exchange energy between the conduction electron and magnetic moment of the ion, J_2, the magnetic moment of the spin of the ions. The condition for formation of spin polaron is that the total energy should be negative, which means that $J_1>J_2$. When $J_1>J_2$, the moments are fully oriented parallel to the direction of conduction electron spins. Well below the transition temperature, the magentic moments are parallel, and the magnetic spins have a comparatively small effect. However, around and above the transition temperature the magnetic moments are randomly oriented, and the contribution of the magnetic spin-polaron coupling becomes more effective. This leads to magnetic polarization of the spin-polaron, so that the system becomes polarized and gives rise to increase of dielectric constant.[35] When the contribution of magnetic spin polaron becomes more effective in the paramagnetic region, the effective mass of the polaron increases. So the activation energy in the paramagnetic phase will be greater. This type of behavior have has been observed in temperature dependent dc conductivity.

In order to verify the existence of magnetic order and to understand the spin dynamics, dc-magnetization measurements as a function of temperature M(T) and magnetic field dependence M(H) have been carried out, as shown in Figure 4. The M(T) measurements have been done in the out-of-plane (magnetic field perpendicular to disc/pellet plane) configuration by PPMS under 100 and 1000 Oe external magnetic field in the temperature range of 300-800 K, as shown in Figure 5(a). The M(T) measurements are recorded at two different modes: zero-field-cooling (ZFC) and field-cooling (FC). CZFO shows a faint bifurcation or hysteresis in M-T data down to 300 K at 100 Oe, which is very common in slightly disordered ferromagnetic systems. However, the bifurcation is smeared out at higher fields of 1000 Oe (as shown in the inset of Figure 5(a)), independent of direction between applied field and disc plane. Usually magnetic FC–ZFC bifurcation signifies the

presence of a magnetic instability (or rather metastability) and can be attributed to spin freeze-out. It indicates the presence of magnetic phase crossover and chemical inhomogeneity in the system.[36,37,38,39,40] From Figure 5(a) it is observed that the magnetization remains nearly constant up to 500 K and above that decreases with increase of temperature and vanishes above ~700 K. In CZFO the estimated ferrimagnetic–paramagnetic transition temperature T_C is around 640 K (+/-10 K) with a broad transition up until 700 K, which reveals the existence of short-range spin interaction. Figure 5(b) shows the magnetic hysteresis M(H) behavior of a CZFO sample at different temperatures up to 40 kOe. It is evident that perfect saturation down to low temperature even for 2 kOe is observed, which a typical signature of ferro/ferrimagnetic behavior. However, a squarer shape develops with increase in temperature. The shapes of the curves show that the initial magnetization rapidly grows in the low-field regime (<2 kOe); however, at high fields the magnetization growth becomes weaker and tends to saturate. The maximum estimated saturation magnetization (M_S) of the sample at 300 K is 119 emu/g and gradually decreases with increase of temperature and completely disappears above 700 K. M(H) curves also show decreases in remnant magnetization (M_r) and coercive field with temperature increase. The observed high M_s and low H_c indicate the soft magnetic nature of CZFO, these soft magnetic nature might be useful for designing of multifunctional devices to switch the magnetization with small external magnetic field.

In conclusion, the observation of large dielectric permittivity with a broad dielectric anomaly near T_N concludes a strong correlation between dielectric and magnetic properties. The origins of high dielectric permittivity have been established. The high dielectric and magnetic properties combined with strong spin-polaron interaction. The ferrimagnetic-paramagnetic phase transition of CZFO has been probed ~640 K, which is well above room temperature. The high dielectric constant, low loss tangent, high T_N with soft magnetic

behavior above room temperature make CZFO an interesting material for possible next generation spintronics and multifunctional device applications.

Acknowledgments

This work was supported by DOE Grant No. # FG02-08ER46526. Dhiren K. Pradhan and Shalini Kumari acknowledge IFN (NSF Grant # EPS - 01002410) for fellowship.

Figure Captions

Fig. 1. (Color online) (a) Rietveld refinement of X-ray diffraction patterns and scanning electron micrograph (inset) of CZFO at room temperature, (b) Three-dimensional schematic sketch of the CZFO unit cell with spinel structure at room temperature.

Fig. 2. (Color online) (a) Representation of the CZFO unit cell along with the FeO_6 octahedral and BO_4 tetrahedral sites, (b) The fitted Raman spectra of pure $CoFe_2O_4$ and CZFO at 300 K with Lorentzian function using Peak-fit program

Fig. 3. (Color online) (a) Temperature dependence of relative dielectric permittivity and loss tangent (inset) with temperatures at different frequencies, (b) The variation of dielectric constant with frequency in a wide temperature range, (c) Complex impedance spectra (Nyquist-plots) at different temperatures, (d) XPS spectra of Fe in CZFO at room temperature.

Fig. 4. (Color online) (a) Frequency dependence of ac conductivity at different temperature, (b) Temperature dependence of n and A with temperature dependence of dc conductivity (inset).

Fig. 5. (a) (Color online) Temperature dependence of magnetization for CZFO measured with zero field cooling (ZFC) and field cooling (FC) with applied field of 100 Oe and 1000 Oe.(inset), (b) M-H hysteresis loops of CZFO at different temperature.

References

[1]Cullity, B. D.; Graham, C. D. *Introduction to Magnetic Materials. 2nd Edition,* Wiley-IEEE Press, 2008.

[2]McCurrie, R. A. *Ferromagnetic materials – Structure and Properties,* Academic Press, San Diego, London, 1994.

[3]Sugimoto, M. The Past, Present, and Future of Ferrites. *J. Am. Ceram. Soc.* **1999,** *82*, 269-280.

[4]Kleemann, W.; Binek, C. *Magnetic Nanostructures.* Springer, 2013, *246*.

[5]Fujimori, H.; Oshimoto, Y. H.; Masumuto, T. Anomalous Eddy Current Loss and Amorphous Magnetic Materials with Low Core Loss. *J. Appl. Phys.* **1981**, *52*, 1893.

[6]Slonczewski, J. C. Initiation of Spin-transfer Torque by Thermal Transport from Magnons. *Phys. Rev. B* **2010,** *82*, 054403.

[7]Bauer, G. E. W.; Saitoh, E.; Wees, B. J. Van. Spin Caloritronics. *Nature Mater.* **2012,** *11*, 391-399.

[8]Eerenstein, W.; Mathur, N. D.; Scott, J. F. Multiferroic and Magnetoelectric Materials. *Nature* **2006**, *442*, 759-765.

[9]Ma, J.; Hu, J.; Li, Z.; Nan, Ce-Wen. Recent Progress in Multiferroic Magnetoelectric Composites: from Bulk to Thin Films. *Adv. Mater.* **2011***, 23,* 1062-1087.

[10]Pradhan, D. K.; Puli, V. S.; Tripathy, S. N.; Pradhan, D. K.; Scott, J. F.; Katiyar, R. S. Room Temperature Multiferroic Properties of $Pb(Fe_{0.5}Nb_{0.5})O_3$–$Co_{0.65}Zn_{0.35}Fe_2O_4$ Composites. *J. Appl. Phys.* **2013**, *114*, 234106.

[11]Pradhan, D. K.; Barik, S. K.; Sahoo, S.; Puli, V. S.; Katiyar, R. S. Investigations on Electrical and Magnetic Properties of Multiferroic $[(1-x)Pb(Fe_{0.5}Nb_{0.5})O_3-xNi_{0.65}Zn_{0.35}Fe_2O_4]$ Composites. *J. Appl. Phys.* **2013**, *113*, 144104.

[12]Ramesh, R.; Spaldin, N. A. Multiferroics: Progress and Prospects in Thin Films. *Nat. Mater.* **2007**, *6*, 21.

[13]Wang, Y.; Hu, J.; Lin, Y.; Nan, Ce-Wen. Multiferroic Magnetoelectric Composite Nanostructures. *NPG Asia Mater.* **2010**, *2*, 61.

[14]Vaz, C. A. F.; Hoffman, J.; Segal, Y.; Reiner, J. W.; Grober, R. D.; Zhang, Z.; Ahn, C. H.; Walker, F. J. Origin of the Magnetoelectric Coupling Effect in $Pb(Zr_{0.2}Ti_{0.8})O_3/La_{0.8}Sr_{0.2}MnO_3$ Multiferroic Heterostructures. *Phys. Rev. Lett.* **2010**, *104*, 127202.

[15]Pradhan, D. K.; Sahoo, S.; Barik, S. K.; Puli, V. S.; Misra, P.; Katiyar, R. S. Studies on Magnetoelectric Coupling in PFN-NZFO Composite at Room Temperature. *J. Appl. Phys.* **2014**, *115*, 194105.

[16]Nan, Ce-Wen.; Bichurin, M. I.; Dong, Shuxiang.; Viehland, D.; Srinivasan, G. Multiferroic Magnetoelectric Composites: Historical Perspective, Status, and Future Directions, *J. Appl. Phys.* **2008,** *103*, 031101.

[17]Mandal, P. R.; Sahu, S.; Nath, T. K. Microstructural, Magnetic, and Electrical Properties of Co–Zn Ferrites Nanoparticles Prepared by Sol–gel Method. *Int. J. Nanosci.* **2011**, 10, 295.

[18]Murthy, S. R.; Rao, T. S. Magnetostriction of Ni-Zn and Co-Zn Ferrites. *Phys. Status Solidi A*, **1985,** *90*, 631.

[19]Nlebedim, I. C.; Vinitha, M.; Praveen, P. J.; Das, D.; Jiles, D. C. Temperature Dependence of the Structural, Magnetic, and Magnetostrictive Properties of Zinc-substituted Cobalt Ferrite. *J. Appl. Phys.* **2013,** *113,* 193904.

[20]Pradhan, D. K.; Puli, V. S.; Kumari, S.; Sahoo, S.; Das, P. T.; Pradhan, K.; Pradhan, D. K.; Scott, J. F.; Katiyar, R. S. Studies of Phase Transitions and Magnetoelectric Coupling in PFN-CZFO Multiferroic Composites. *J. Phys. Chem. C.* **2016**, *120*, 1936.

[21]Kittel, C. *Introduction to Solid State Physics*, *8th Edition*, John Wiley & Sons, Inc, 2004.

[22]Zheng, H.; Weng, W.; Han, G.; Du, P. Colossal Permittivity and Variable-Range-Hopping Conduction of Polarons in $Ni_{0.5}Zn_{0.5}Fe_2O_4$ Ceramic. *J. Phys. Chem. C*. **2013**, *117*, 12966.

[23]Pradhan, D. K.; Misra, P.; Puli, V. S.; Sahoo, S.; Katiyar, R. S. Studies on Structural, Dielectric, and Transport Properties of $Ni_{0.65}Zn_{0.35}Fe_2O_4$. *J. Appl. Phys.* **2014**, *115*, 243904.

[24]Chen, D. G.; Tang, X. G.; Liu, Q. X.; Jiang, Y. P.; Ma, C. B.; Li, R. Impedance Response and Dielectric Relaxation in Co-precipitation Derived Ferrite $(Ni,Zn)Fe_2O_4$ Ceramics. *J. Appl. Phys.* **2013,** *113*, 214110.

[25]Verma, A.; Thakur, O. P.; Prakash, C.; Goel, T. C.; Mendiratta, R. G. Temperature Dependence of Electrical Properties of Nickel-Zinc Ferrites Processed by the Citrate Precursor Technique. *Mater. Sci. Eng. B* **2005,** *116*, 1.

[26]Lunkenheimer, P.; Fichtl, R.; Ebbinghaus, S. G.; Loidl, A. Nonintrinsic Origin of the Colossal Dielectric Constants in $CaCu_3Ti_4O_{12}$. *Phys. Rev. B.* **2004,** *70*, 172102.

[27]Gopalan, E. V.; Malini, K. A.; Saravanan, S.; Kumar, D. Sakthi; Yoshida Y.; Anantharaman, M. R. Evidence for Polaron Conduction in Nanostructured Manganese Ferrite. *J. Phys. D. Appl. Phys.* **2008**, *41*, 185005.

[28]Chen, W.; Zhu, W. ; Tan, O. K.; Chen, X. F. Frequency and Temperature Dependent Impedance Spectroscopy of Cobalt Ferrite Composite Thick Films, *J. Appl. Phys.* **2010,** *108*, 034101.

[29]Wagner, C. D.; Riggs, W. M.; Davis, L. E.; Moulder, J. F.; Muilenberg, G. E. *Handbook of X-ray Photoelectron Spectroscopy*, Perkin-Elmer Corp., Physical Electronics Division, Eden Prairie, MN, 1979.

[30]Jonscher, A. K. The `universal' dielectric response. *Nature (London)* **1977,** *264*, 673.

[31]Lu, Z.; Bonnet, J. P.; Ravez, J.; Hagenmuller, J. P. *Sol. St. Ionics* **1992,** 57, 235.

[32]Elliot, S. R. A.C. Conduction in Amorphous Chalcogenide and Pnictide Semiconductors. *Adv. Phys.* **1987,** *36*, 135.

[33]Ortega, N.; Kumar, A.; Bhattacharya, P.; Majumder, S. B.; Katiyar, R. S. Impedance spectroscopy of multiferroic $PbZr_xTi_{1-x}O_3/CoFe_2O_4$ layered thin films. *Phys. Rev. B* **2008***, 77*, 014111.

[34]Barick, B. K.; Mishra, K. K.; Arora, A. K.; Choudhary, R. N. P.; Pradhan, D. K. Impedance and Raman spectroscopic studies of $(Na_{0.5}Bi_{0.5})TiO_3$ *J. Phys. D: App Phys.* **2011,** *44*, 355402.

[35] N. F. Mott, Metal-Insulatro transtions, Taylor & Francis, Newyork, 1990, Page 1992

[36]Joy, P. A.; Kumar, P. S. A.; Date, S. K. Origin of the Cluster-glass-like Magnetic Properties of the Ferromagnetic System $La_{0.5}Sr_{0.5}CoO_3$. *J. Phys. Cond. Mat.* **1998**, *10,* 11049.

[37]Ghosh, B.; Kumar, S.; Poddar, A.; Mazumdar, C.; Banerjee, S.; Reddy, V. R.; Gupta, A. Spin Glasslike Behavior and Magnetic Enhancement in Nanosized NiZn Ferrite System. *J. Appl. Phys.* **2010,** *108*, 034307.

[38]Li, X.–G.; Fan, X. J.; Ji, G.; Wu, W. B.; Wong, K. H.; Choy, C. L.; Ku, H. C.; Field-induced Crossover from Cluster-glass to Ferromagnetic State in $La_{0.7}Sr_{0.3}Mn_{0.7}Co_{0.3}O_3$. *J. Appl. Phys.* **1999**, *85***,** 1663.

[39]Karmakar, D. S.; Mandal, K.; Kadam, R. M.; Paulose, P. L.; Rajarajan, A. K.; Nath, T. K.; Das, A. K.; Dasgupta, I.; Das, G. P. Ferromagnetism in Fe-doped ZnO Nanocrystals: Experiment and Theory. *Phys. Rev. B.* **2007**, *75*, 144404.

[40]Borkar, H.; Choudhary, R. J.; Singh, V. N.; Tomar, M.; Gupta, V.; Kumar, A. Competing magnetic interactions and low temperature magnetic phase transitions in composite multiferroics. *Mater. Res. Express* **2015**, *2*, 086101.

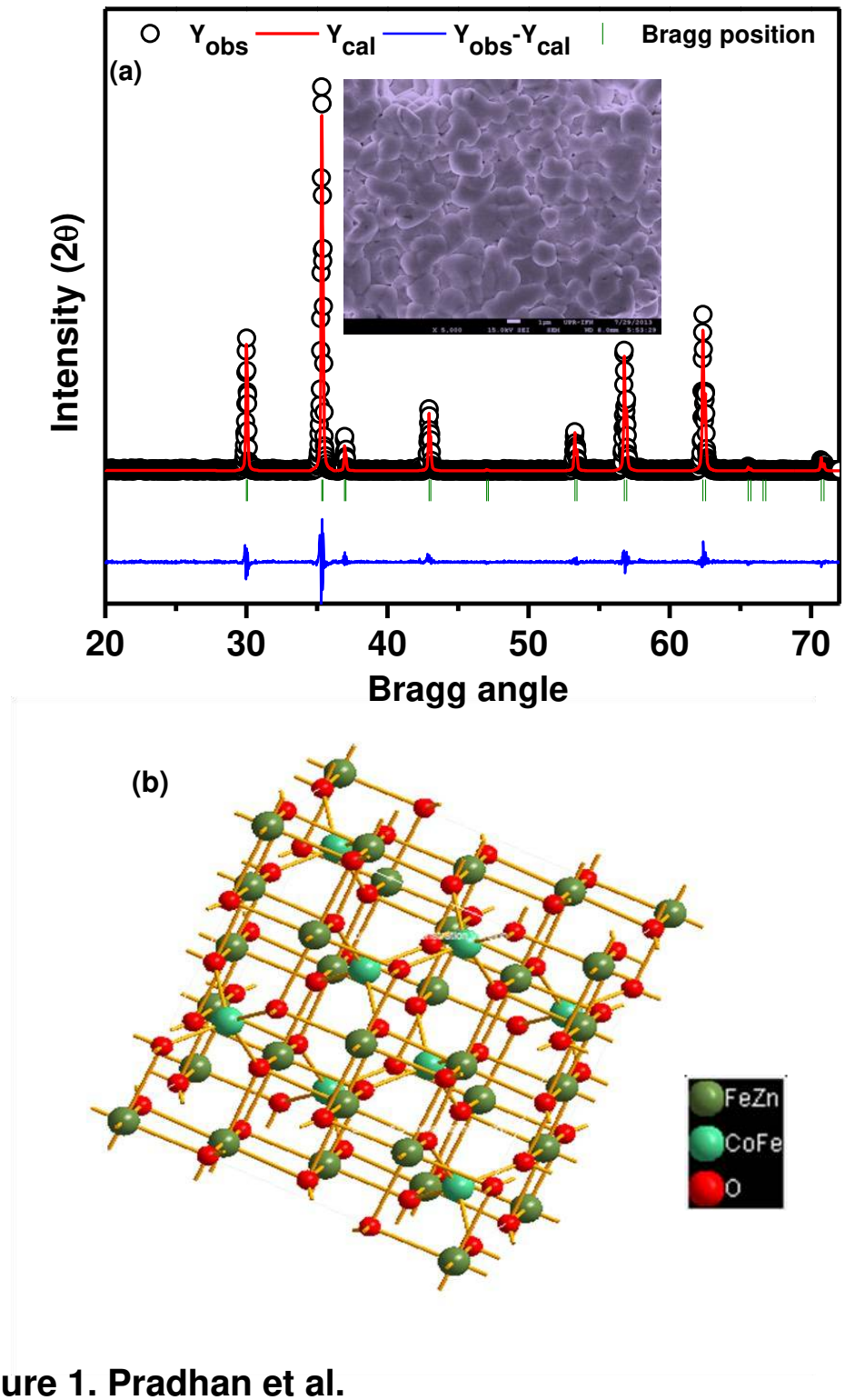

Figure 1. Pradhan et al.

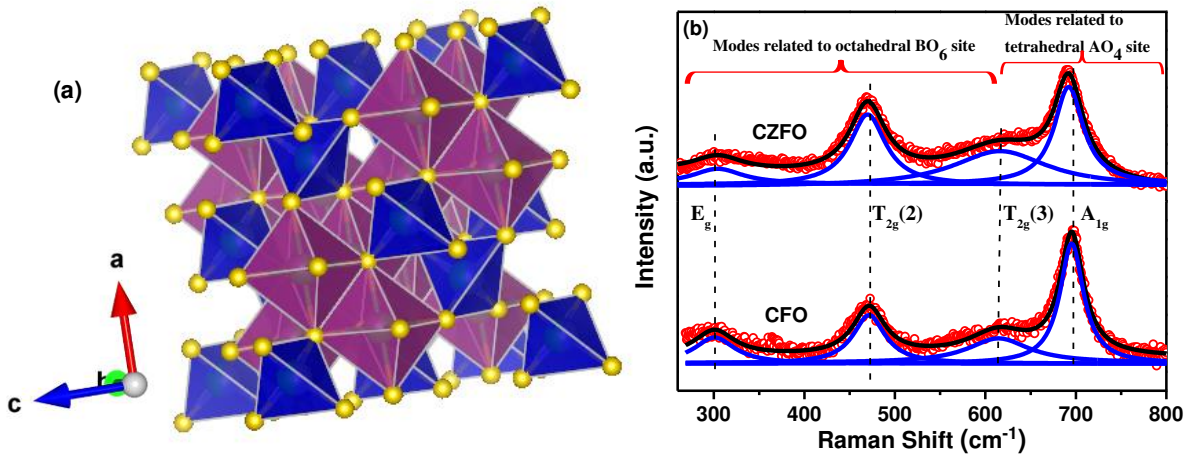
(a)
a
c
(b)
Modes related to octahedral BO6 site
Modes related to tetrahedral AO4 site
CZFO
CFO
Eg
T2g(2)
T2g(3)
A1g
Intensity (a.u.)
300
400
500
600
700
800
Raman Shift (cm-1)

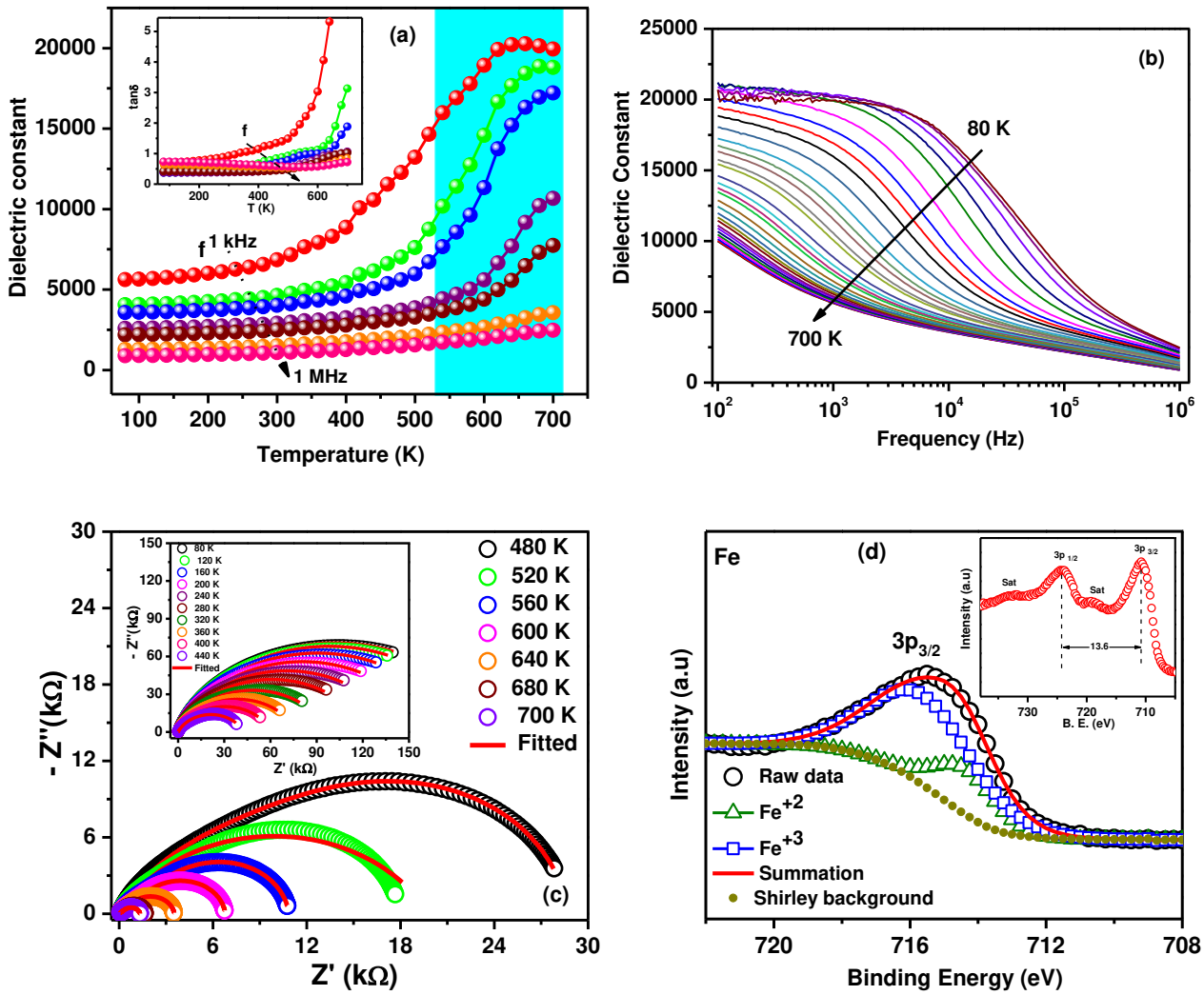

Figure 3. Pradhan et al.

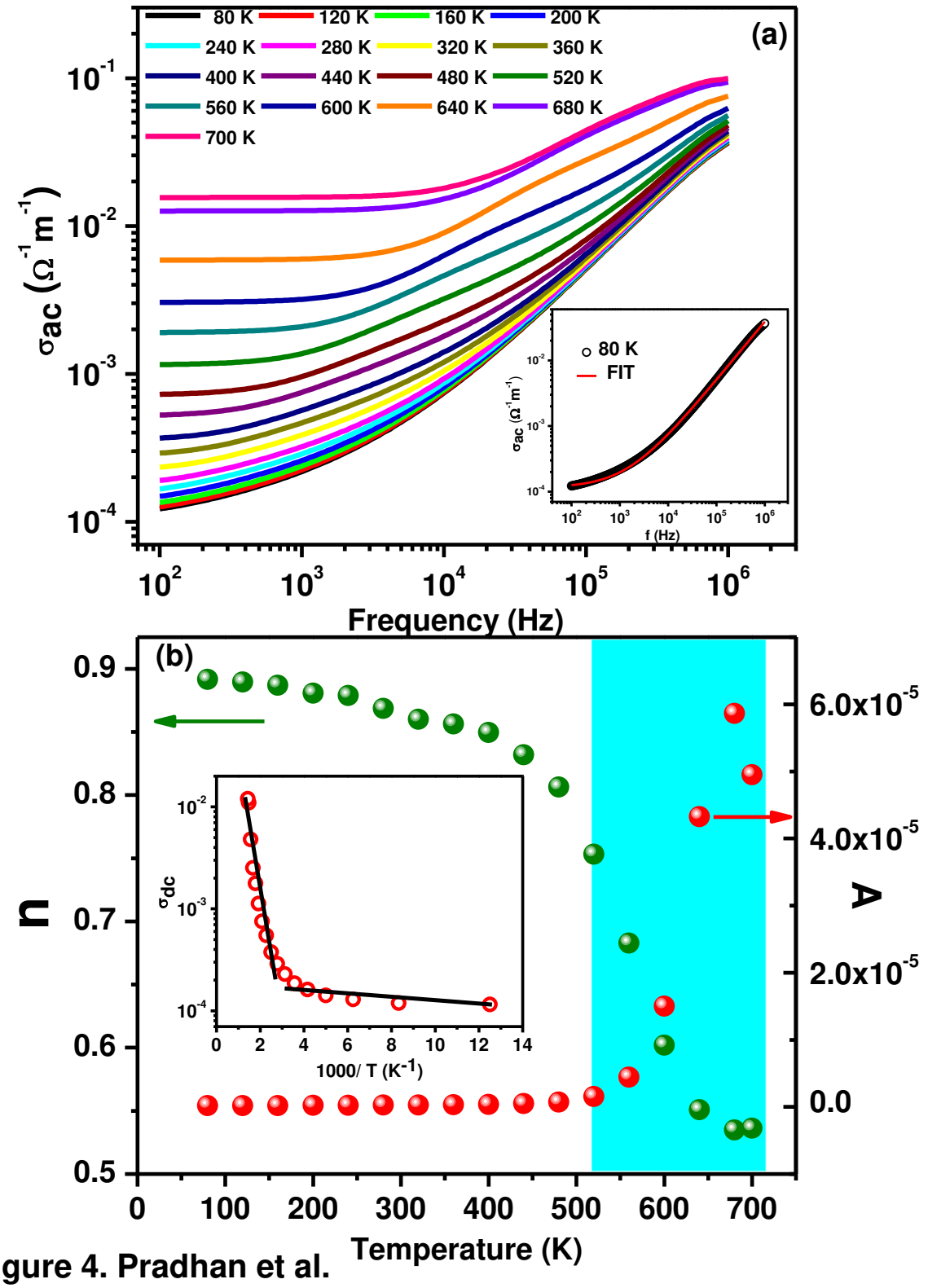

Figure 4. Pradhan et al.

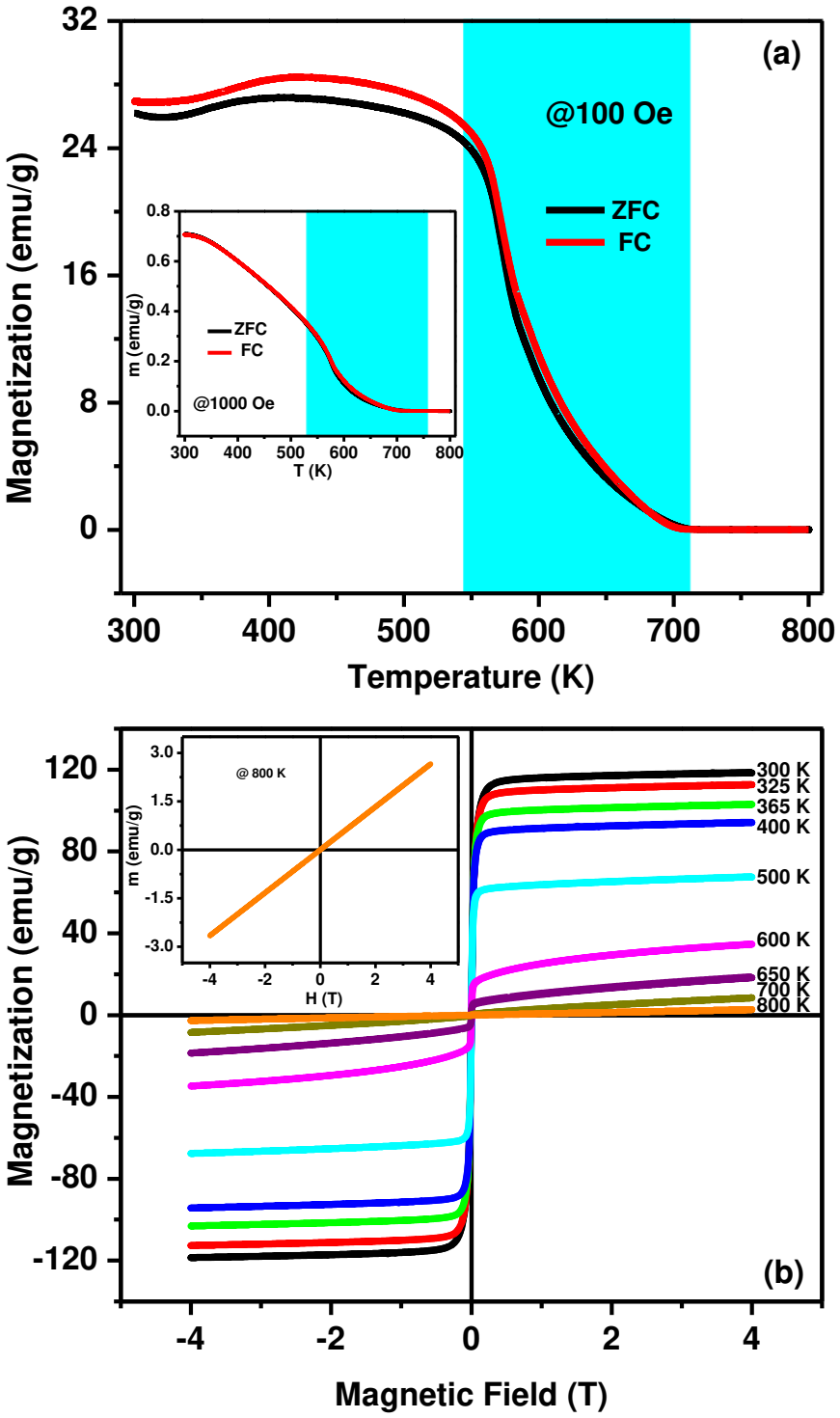

Figure 5. Pradhan et al.